SSRG International Journal of Mechanical Engineering
ISSN: 2348-8360/ https://doi.org/10.14445/23488360/IJME-V13I3P103

Volume 13 Issue 3, 34-43, March 2026

Original Article

Experimental Study of Nickel Electroplating and CuO Nanocoolant on Corrosion Rate and Hardness of ASTM A36 Steel

Firda Herlina[1], Yuli Panca Asmara[2], Januar Parlaungan Siregar[3], Ahmad Janan Febrianto[4], Syamsul Maarif[4], Andi Ibrahim Soumi[4], Anhar Khalid[5], Sugiman[6]

[1]*Islamic University of Kalimantan Muhammad Arsyad Al Banjari Banjarmasin, South Kalimantan, Indonesia.*
[2]*INTI International Universiti, FEQS, Negeri Sembilan, Malaysia.*
[3]*Faculty of Mechanical and Automotive Engineering Technology (FTKMA), Universiti Malaysia Pahang, Al-Sultan Abdullah, 26600 Pekan, Pahang, Malaysia.*
[4]*Mechanical Engineering, Sarjanawiyata Tamansiswa University, Indonesia.*
[5]*Politeknik Negeri Banjarmasin.*
[6]*Mechanical Engineering Faculty, Mataram University.*

[1]*Corresponding Author : tanyafirda@gmail.com*

Received: 18 December 2025 Revised: 20 January 2026 Accepted: 19 February 2026 Published: 28 March 2026

Abstract *- ASTM A36 carbon steel is widely used as an alternative type of steel for the manufacturing and construction industry, but the poor corrosion resistance and relatively low surface hardness of the steel result in low performance in long-term operation. Therefore, manufacturing innovation is required to obtain high coating performance. In this article, ASTM A36 steel for material is obtained, in the method of enhancing surface properties with nickel electroplating and CuO nanocoolant diffusion at 0.25%, 0.5%, and 0.7% concentrations. Surface hardness was the established method of Vickers hardness testing, while the corrosion behavior of the ASTM A36 was measured with weight-loss immersion tests in HNO_3, H_2SO_4, and HCl solutions. The coating morphology and elemental distribution are explored by Scanning Electron Microscopy (SEM) and Energy-Dispersive X-ray spectroscopy (EDX). Quantitatively, the uniformity of coatings was evaluated by looking at the mean, standard deviation, and CV of elemental composition. The results show that there are significant improvements in surface performance with the ratio of CuO concentration. Hardness increased by ca 9%; however, the highest hardness was recorded at 0.7% CuO. Corrosion test with acidic environment indicated a decrease in weight loss because the corrosion rate of 0.25–0.5% was reduced, and more effective protection can be obtained by 0.7% CuO. The EDX results showed that the coating containing 0.7% CuO had a greater elemental homogeneity, with CV <50%, and coatings containing low CuO had a significant inhomogeneity. SEM data confirmed that the 0.7% CuO coating created a deep, uniformly dense, and uninterrupted layer with a low level of porosity and agglomeration of the nanoparticles, which contributed to enhanced corrosion resistance. Ni–CuO coatings showed better corrosion resistance and microstructural uniformity due to homogeneous nanoparticle dispersion, outperforming conventional and reported coatings.*

Keywords *- ASTM A36 steel, Nickel electroplating, CuO nanoparticles, Corrosion behavior, Surface hardness, Microstructural analysis.*

1. Introduction

ASTM A36 low-carbon steel is the most widely used steel in structural and commercial applications, as it has sufficient mechanical performance for relatively little cost. Its yield strength is greater than 250 MPa, and its tensile strength is between 400 and 550 MPa, which indicates that it is the ideal device for both a strengthening and ductile construction process [1]. This phenomenon accounts for the heavy usage of the material in construction, factory, and energy industries. But this material also poses its own challenges, with its own performance problems that keep it from functioning well in harsh service environments. This one-dimensional shape of surface steel also has a series of serious disadvantages, due to its relatively low corrosion resistance and relatively moderate hardness resistance. Under the hostile acidic systems and high chlorine ions of such a steel, the weaknesses are magnified. In that type of operating, an electrochemical reaction is produced naturally at the steel surface, and material reduction can be achieved, and surface deterioration can be increased in a brief time [2, 3]. Prolonged exposure causes the corrosion cells to accumulate at a gradual rate, which weakens the structure and hence decreases the service life, and the cost increases for frequent maintenance and rapid part replacement. Surface remediation schemes, including organic protective coatings, metal treatment, and chemical conversion, have been developed to address these issues in natural conditions. Nickel-type coating, including Ni-type coating and other

electroplating processes, is the most common; as a result, the technology has increased the surface hardness, wear resistance, corrosion protection, and corrosion resistance of many low-carbon steels. These deposited nickel layers provide the same protection, and at the same time prevent the effect caused by different toxic species and reduce the electrochemical activity of the steel surface as well.

Conventional nickel coatings are widely used for corrosion protection; however, under highly aggressive environments, they often develop microstructural defects such as pores, microcracks, and compositional non-uniformity. These defects act as pathways for corrosive media, triggering localized corrosion and reducing long-term reliability [5]. Recent advances in nanomaterials have introduced metal oxide nanoparticles, particularly CuO, due to their chemical stability and ability to promote dense coating structures. Although previous studies report improved mechanical and general corrosion properties with nanoparticle addition, limited research has systematically examined how CuO incorporation mitigates microstructural defects and enhances resistance to localized corrosion in severe environments. Therefore, this study investigates the effect of CuO nanoparticles on microstructure refinement, porosity reduction, and corrosion performance of Ni-based coatings to clarify their role in improving coating durability. This mixture is targeted to be able to block negative ions, such as chlorides, from being transported, increasing corrosion resistance under harsh conditions [6, 7]. And so, the composite coatings of Ni-CuO are increasingly popular materials for the service life extension of low-carbon steel products.

The effect of exposure to stress on the coating performance of the CuO nanoparticle system of a coating system by copper cobalt, nickel carbide, copper cobalt nanoparticles, due to the increased load and the homogenization of the dispersion distribution in the deposited morphology, with extremely high sensitivity, depends heavily on the amount of load and the deposition of this coating system. In the case of weak CuO concentration, the concentration distribution is asymmetric, and nanoparticles cannot act as a protective network and resist corrosion stress. However, CuO concentration over-exposure could be highly porous, which localizes the porosity and micro-galvanic interactions for the small clusters of CuO and steel substrate. Such a tendency may favor a localized type of corrosion instead of a moderate level one [8]. As a result, the ideal compromise between CuO concentration content, coatings homogeneity, surface hardening, and corrosion resistance continues to be a most important challenge in nanocomposite coating systems. Previous studies indicated that the electroplating performance of nickel coating methodologies can be enhanced considerably by doping CuO nanoparticles [9], while this is largely attributed to the particle compositions and dispersion quality.

A reduction in corrosion rates of more than 50 times greater than the unmodified ones was achieved for zinc phosphate coatings modified with CeO_2-CuO nanocomposites, which demonstrates the extensive inhibition effect of CuO-based additives [10]. In addition, composite coating with CuO nanoparticles combined with the corrosion abatement mechanism can be a valuable improvement in the protection against corrosion and antibiofouling effect of mild steel. The addition of CuO nanoparticles also enhances the mechanical performance and corrosion resistance of mixed metallic coating systems significantly. Thao et al. [11] also proved the polarization behavior of nickel electrodeposition that led to coating morphological modification, and the properties of deposit quality were improved by CuO and CeO_2 nanoparticles. Similarly, Barsana et al. [12] observed that CeO_2–CuO nanocomposites-modified zinc phosphate coatings produce a more stable and better-packed layer of carbon steel with 50 times lower corrosion rate.

Moreover, D'Acosta et al. [13] reported that similar improvements in performance have been achieved in CuO-based hybrid zinc coatings, green SiO_2–CuO nanocoatings [14], plasma electrolytic oxidation coatings for aluminum alloys [15], and various polymeric protective coatings [16, 17]. CuO nanoparticles exhibited well-characterized protective activity; their protective action, their protection effect, and the presence and distribution were established. If they are at low amounts of CuO, then they produce a very weak coating with very little or poor distribution, though their excessive contents result in their particle aggregation and weakness of coating structure, and a tendency towards local corrosion.

Therefore, good control not only of CuO loading but also of the deposition of the same kind is needed to obtain the surface hardness and corrosion resistance. The major reference papers on optimization are shown in Table 1.

Table 1. Different types of higher hardness and less corrosion of CuO-based coating systems

Studies	Substrate	CuO additive (or related nanocomposites)	Hardness	Corrosion rate
CeO_2–CuO nanocomposite in ZnP layer	Mild steel, zinc phosphate coating	CeO_2–CuO nanocomposite (0.3–0.9 g·L^{-1})	Hardness increases from 153.7 HV to 173.8 HV at 0.9 g·L^{-1}	Corrosion rate decreased from 1.843 mm/y to 0.036 mm/y with CeO_2–CuO nanocomposite [10]
Ag-CuO/epoxy hybrid nanocomposite	Copper substrate, epoxy coating	5.0 wt% Ag–CuO	Polarization shows a significant increase	Corrosion rate decreased to ~3.81×10^{-4} mm/y, >99%

				reduction compared to uncoated.[18]
CuO in micro-arc oxidation/PU composite	Magnesium alloy	CuO nanoparticles (micro-arc distribution)	-	$I_{(corr)} \approx 7\times10^{-9}$ A/cm² indicates very high corrosion resistance [19].
Cu-Ni-ZnO:Ni: CuO nanocomposite coating	Cu-Ni alloy (coating)	Zn (0.96), Ni (0.02), Cu (0.02) O nanoparticles	Maximum hardness up to ~558 HV [19].	A low $I_{(corr)}$ of $\approx2.21\times10^{-3}$ mA/cm² indicates increased corrosion resistance [19].

2. Examination Methods

2.1. Nanocoolant Preparation and Immersion Procedure

CuO nanocoolant solutions were prepared by dispersing copper oxide (CuO) nanoparticles in distilled water at concentrations of 0.25 wt%, 0.5 wt%, and 0.75 wt%, corresponding to 2.5 g/L, 5.0 g/L, and 7.5 g/L, respectively, in a total solution volume of 500 mL. The nanoparticle suspensions were mechanically stirred to ensure uniform dispersion prior to use. Cylindrical ASTM A36 steel specimens (10 mm diameter × 10 mm height) were used as substrates. All experiments were conducted at laboratory temperature and atmospheric pressure. Nickel electroplating was performed using a nickel-based electrolyte system with a power input of 25 W and an electrolyte volume of 500 mL. After electroplating, the coated specimens were subjected to passive immersion in the prepared CuO nanocoolant solutions for post-treatment modification. Based on the treatment conditions, the samples were divided into four groups: (i) untreated raw material, (ii) Treatment A (Ni plating + 0.25 wt% CuO), (iii) Treatment B (Ni plating + 0.5 wt% CuO), and (iv) Treatment C (Ni plating + 0.75 wt% CuO).

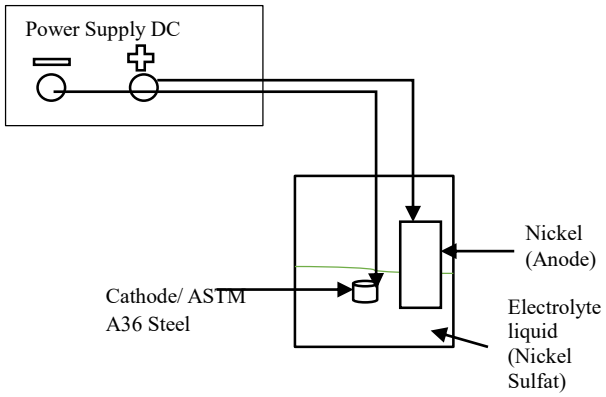

Fig. 1 The electroplating process is illustrated in a schematic experimental setup

2.2. Corrosion Test Setup

Corrosion was performed according to ASTM G31 standard [20, 21]. Cylindrical ASTM A36 steel specimens were manufactured of similar scales and washed off, dried, and weighed to serve as a preliminary mass test on an analytical balance. The immersion corrosion analysis was carried out on three commercially available acidic media (hydrochloric acid (HCl, 32%), sulfuric acid (H_2SO_4, 95%), and nitric acid (HNO_3, 65%)), containing solution volumes of 300 mL for three test tubes. These tests were conducted to test the influence of surface treatments on ASTM A36 steel corrosion behavior. Samples were taken for specimens and removal of corrosion products with a suitable chemical cleaning solution at the end of the immersion. The samples were then placed in deionized water and alcohol, washed, dried, and measured to determine their estimated mass. Corrosion rate was calculated by weight loss at the exposed area, time in water, and the density of the material. They adopt ASTM G31 equations [22] (Equation (1) to estimate the mass loss and the corrosion rate.

$$\text{Weight Loss} = (W_0-W_1)/W_0 \quad (1)$$

Where:
W_0 = initial weight of specimen (g). W_1= final weight of specimen (g).

2.3. Vickers Hardness Test

The surface hardness of ASTM A36 steel after nickel electroplating and CuO nanoparticle diffusion was calculated from the Vickers method as determined by ASTM E384. All specimens were ground and polished homogenously to a polished surface without observable scratches before testing. The hardness was measured according to the diamond pyramidal indenter, face angle 136°.

The thickness of the coating material resulted in the applied load on the samples and duration (average duration between 10 and 15 s). After indentation, the two diagonal lengths (d_1, d_2) were measured under an optical microscope, and averaged using equation (2)/the mean is calculated as Vickers Hardness Value(HV) [23]. All these measurements were performed in a variety of locations in order to create a consistent result from the samples, and were in the center region and the periphery region of the specimen, respectively. The hardness figures are the average of these measurements and are represented as the Standard Deviation.

$$HV=(1.854\times F)/d^2 \quad (2)$$

2.4. Characterization

SEM–EDX measurements were performed at eight randomly assigned locations on each sample to estimate the coverage structure of various layers of the coating material. Average elemental concentrations of these samples were used to calculate the mean composition values. The regularity of the elemental distribution was also verified using various statistical infrastructures - SD and CV. The CV was used in this study as a quantitative parameter for uniform coating homogeneity; low CV was correlated with a higher fraction of uniform elemental concentration across the surface [24, 25].

3. Result and Discussion

3.1. Corrosion Process in Acid (HNO_3, H_2SO_4, HCl)

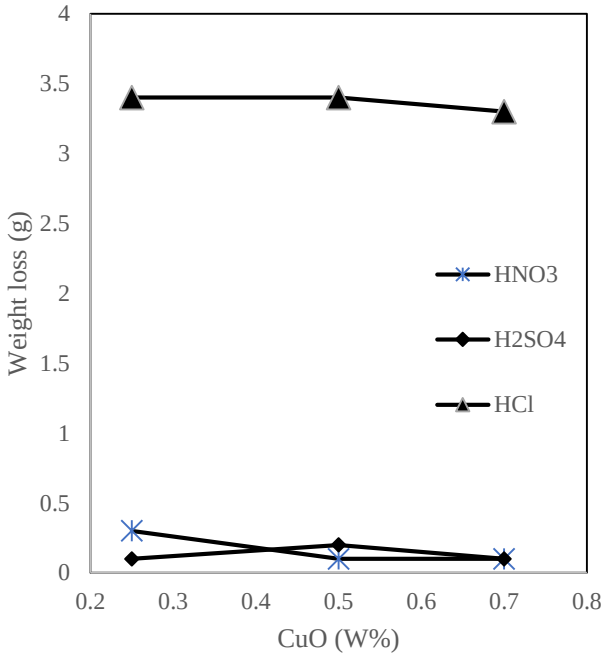

Fig. 2 Influence of CuO content in ASTM A36 in different acid solutions

From the analyzed weight loss result, it has been reported that the corrosion resistance of nickel coating on ASTM A36 steel, together with CuO nanocoolant, is mainly attributable to CuO contents. The characteristic of the two is indicated by the chemical content of the CuO and the pH setting of the two products, as shown in Figure 2. The addition of CuO NPs in all of the test solutions caused a material loss attenuation from 0.25 to 0.5 times the corrosion rate. The highest performance was improved at the CuO dose of 0.75 wt%.

The biggest change in weight loss between all CuO concentrations was observed above high intensity (~3.3–3.4 g) concentration towards HCl, confirming the chloride ions in HCl that are highly corrosive. The apparent reduction in size reduction seen at 0.75 wt% CuO was only slight; in effect, the protection was stronger at high nanoparticles (0.75 wt%) compared to 0.5 wt%.

In contrast, for H_2SO_4 and HNO_3, the weight loss was extremely low compared to that of HCl, implying less drastic corrosion. The results showed the presence of more mass reduction for 0.25 wt% CuO coatings than for 0.5 and 0.75 wt%, which suggests that a protective surface should be obtained from more nanoparticles. At 0.75 wt% CuO, this results in higher surface coverage and less passage for this highly permeative ion to penetrate through the surface coating of the active ion. Overall, the results establish that alloying with nickel for electroplating and optimal combining for optimal CuO nanocoolant enhances corrosion resistance even more [25], particularly when the solvent conditions are acidic, absent, or with few chloride ions.

3.2. Hardness Test

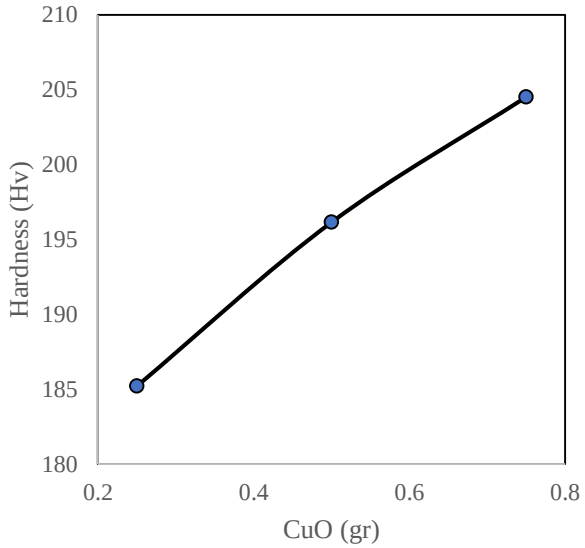

Fig. 3 Effect of CuO concentration on the hardness of ASTM A36 metal after electropolishing

ASTM A36 steel Vickers hardness was also increased when CuO was added. The hardness at 0.25 g CuO was 185.21 HV, 196.15 HV at 0.5 g, 204.51 HV at 0.75 g, implying that CuO is likely to act as a stabilization agent for steel reinforcement, by restraining dislocation motion and increasing the electroplated film density. Above and above to further increase the resistance to plastic strain for the surface, more reinforcing particles will probably aggregate on its surface in a higher concentration of CuO, which will result in stronger hardness. If the maximum hardness is set at 0.75 g CuO, this indicates that the density is higher and a solid surface layer. The small size and tight confinement in HCl will restrict the influx of aggressive ions (e.g., chloride ions, [Cl^-] particles) and facilitate the formation of a larger protective layer. Some corrosion tests, however, were equivalent or slightly worse than untreated steel and showed a significant corrosive effect of HCl on low-carbon steel. Nonetheless, the hardness values of CuO-contributing samples (0.25 g and 0.5 g) obtained were significantly lower as a result of irregular surface microstructure composition. This seemed to have an effect on the uneven spatial distribution of CuO and agglomeration of particles, and increased porosity of the electroplated layer. However, the intrinsic inhomogeneities from the CuO phase to the steel substrate could promote microgalvanic cells, which could promote local corrosion. The mechanical strength and corrosion resistance of CuO nanoparticles are enhanced after their dispersion is as complete and uniform as it can be, and a continuous surface layer is formed [27].

3.3. Chemical Composition

Table 2 shows significant differences in the concentration of each of the CuO densities by quantitative EDX and the weight percent difference between Ni, Cu, and O intensity. These are the relative quantities that each element will be present in the surface of the material. Consistency between Cu and O enables well-distributed CuO, while the decrease in Ni intensity represents nickel.

Conversely, non-homogenized distribution patterns, e.g., an increase in Cu and O content of coatings, imply particle agglomeration and voids in CuO coatings. Results: The surface of the layer is relatively uniform at 0.25 g; at 0.5 g CuO, the distribution of CuO is irregular, but at 0.75 g of CuO, the formation of substantial agglomeration is taking place, preventing the rest of the CuO layer from going on top of the surface. The Ni–CuO coatings worked better than previous methods because the nanoparticles spread evenly, filling pores and cracks, making the coating denser and more resistant to corrosion.

Table 2. Average EDX test results of chemical elements in test materials

Element Symbol	Element Name	CuO (gr)			
		0	0.25	0.5	0.7
C	Carbon	65,764	59,457	24,924	44,443
O	Oxygen	2,273	8,991	0.279	34,171
Na	Sodium	0.452	0.000	0.000	0.846
Si	Silicon	0.092	0.186	0.477	0.154
Cl	Chlorine	0.000	0.000	0.252	0.606
Fe	Iron	31,122	31,098	73,195	3,656
This	Nickel	0.133	0.267	0.381	14,548
Cu	Copper	0.164	0.000	0.492	1,031

3.4. Microstructure Analyses

Figures 4-7 show the results of SEM observations, and EDX analyses were performed to reveal the surface morphological characteristics and distribution of chemical elements in ASTM A36 steel coated with nickel (Ni) and electropolished at different CuO concentrations (from 0.25 g to 0.7 g). 0 CuO.

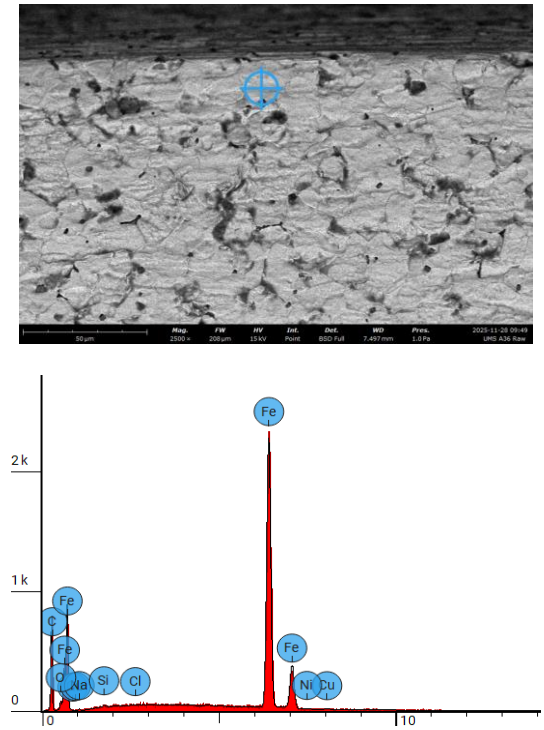

Fig. 4 SEM images and EDX of ASTM A36 steel with nickel (Ni) coating

SEM images demonstrate that the A36 surface and cross-section microdamage have become more extreme. A rough surface, a large area of open pores, microcracks, and a loose matrix structure can be seen. Grain boundaries can be clearly seen and are unprotected, indicating that the substrate has encountered an aggressive environment (Figure 4).

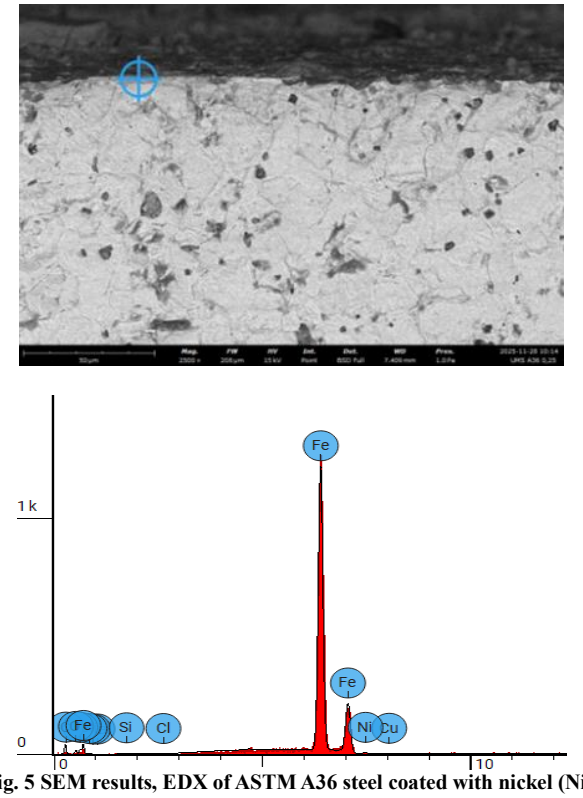

Fig. 5 SEM results, EDX of ASTM A36 steel coated with nickel (Ni), electropolished with CuO (0.25 g)

In Figure 5, the thin electroplated layer shows thinness and discontinuity when 0.25 g of CuO is put on top as well. It consists of many pores, not uniform particles, and the microstructure consists of well-defined grain boundaries.

Other areas, which have been shown with a high concentration in the Fe–Ni matrix, in addition to not being adequately protected by CuO, mean that there is not enough protection of CuO in this shape that is equivalent to a homogeneous protective network. This corresponds with the EDX data with high CV, low homogeneity, and fluctuating CuO distribution.

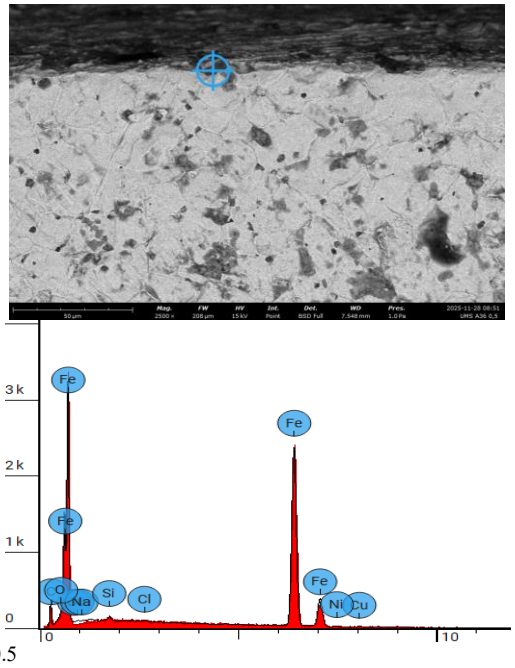

Fig. 6 SEM and EDX of an ASTM A36 steel coated with nickel (Ni) by electropolishing, prepared with 0.5 g CuO concentration

Following exposure to 0.5 g CuO, the surface layer thickens to the limit of 0.25 g, but the morphology is highly CuO agglomerating (Figure 6). This involves dark and bright patches, microcrack development, and local particle deposition, with the observed presence of a highly scattered distribution of CuO without any standardization. Therefore, even though local inhomogeneity arises, the Cu and O quantities rise quantitatively due to this agglomeration. This coincides with SD and CV values at the highest for 0.5 g of all compositions, which are the highest-microstructure unstable at 0.5 g conditions.

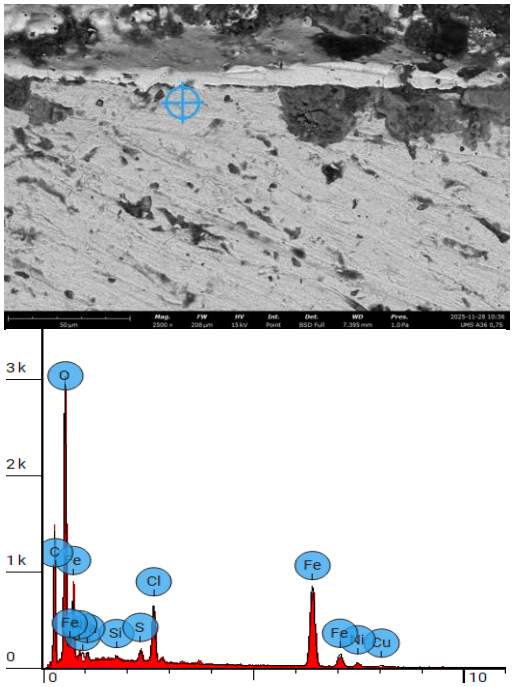

Fig. 7 Results of SEM and EDX analysis of nickel (Ni)-coated ASTM A36 steel and the subsequent electropolishing with CuO (0.7 g concentration).

Figure 7 indicates that the coating was clearly morphology enhanced in the presence of 0.7 g CuO. They appear to be more uniform, more contiguous, and more adherent to the A36 substrate. By regulating the volume of pores and the agglomeration, the distribution of CuO particles was relatively constant compared to 0.5 g, but while the local differences of oxygen were plainly visible, the coating structure was reasonably stable. After that, we can deduce that Cu has the smallest (CV) variation toward other compositions as compared to those taken from the EDX analysis, for which a smaller range was observed at the 0.7 g content, which indicates a less heterogeneous copper distribution. The corrosion rates reflect surface morphology.

3.5. Analysis of Corrosion Rate vs Surface Morphology

Surface morphology is another important parameter regarding the corrosion reaction time of the material in an HCl medium [27, 28]. In SEM images of nickel-electroplated ASTM A36 steel, it is exhibited in large-scale microdamage with roughness, many open pores, microcracks, and loose matrix structure. Uncovered grain boundaries represent what is exposed directly to the corrosive material. The rapid diffusion of corrosive ions (H^+ and Cl^-) leads to rapid corrosion and deterioration of the material since no continuous protective layer is placed. As a result of these localized corrosion, pits of porosity and microcracks form that lead to the dissolution of the metal and the degradation of the structural integrity of the substrate [30]. Such a high corrosion rate and unmoderated elemental distribution is similar to that in electrochemical paired with EDX analysis at untreated samples. Morphology improvements were also only appreciable at a decrease of 0.25 and 0.5 g of CuO addition (Figures 5 and 6). They have thin, discontinuous, and porous coatings, with uneven scattering of CuO particles. In previous works, this behaviour was exhibited [8], with insufficient loading of nanoparticles and poor coverage resulting in limited surface area of species to prevent corrosion through aggregation and loss of complete layer development. Thus, the Fe–Ni matrix was dominant, even though the corrosion rates were higher, where aggressive ions (H^+ and Cl^-) can overcome the defects and pores of the structure. On the contrary, a significant enhancement in the coating morphology and corrosion resistance occurred with the initial 0.7 g content of CuO (Figure 7**)**. The coating was visibly dense and continuous, though in terms of the ASTM A36 substrate, there was better conformance. At the same concentration, the CuO nanoparticles were better dispersed in the matrix of microvoids, and this reduced the porosity and agglomeration observed [21]. Such conductability is in accordance with the data, which document that ideal particle loading results in better compact microstructures and benefits the coating structure [6, 18]. While the coating structure was stable and had some fluctuations in oxygen due to mixing, 0.7 g presented relatively homogeneous Cu content, confirming that EDX composites are the most homogeneous in their composition. This homogeneity triggered a sharp decrease in corrosion rate; the homogenizing dispersion of nanoparticles successfully

inhibited the path of ionic diffusion and localized pathways of inflammation starting corrosion [31]. As a result, the exceptional corrosion resistance at the concentration of 0.7 g CuO is believed to be the result of the co-benefits resulting from the increased micro-structural compactness and enhancement of CuO dispersion, and due to the strong barrier characteristics of the electroplated coating.

3.6. Homogeneity Analysis

Homogeneity of the coating was quantitatively measured with mean, Standard Deviation (SD), and Coefficient of Variation (CV) calculated by EDX measurements obtained at eight locations of a known sample surface selected randomly. The method of SD and CV in checking the homogeneity of the distribution of elements is two measures of homogeneity in each case for SD and CV (Equations 3 and 4). In this case, a lower SD is equivalent to a homogeneous coating.

3.7. Standard Deviation

Standard Deviation is defined as the statistical measure of how widely the data is spread in the direction of the average value (mean) [24, 25]. Small SD → clustered data around the mean → more uniform/homogeneous. Large SD → data is distributed far from the mean → not homogeneous. Mathematically:

$$SD = \sqrt{\frac{\sum(x_i - \bar{x})^2}{n-1}} \quad (3)$$

In EDX analysis, SD is the difference in element concentration from one point to the next in the analysis of measurement points.

Small SD values indicate evenness in the element distribution/agglomeration.

3.8. Coefficient of Variation

The coefficient of variation is a relative measure of data spread as a percentage of the mean (see also 25, 26).

$$CV = SD/Mean \times 100\% \quad (4)$$

General Interpretation of CV

CV < 20% → very homogeneous. 20–50% → moderate homogeneity. 50–100% → not homogeneous. >100% → very heterogeneous. Table 3 shows average Standard Deviation (SD) and Coefficient Of Variation (CV) values of the elements observed from the workpiece samples subject to treatment with varying concentrations of CuO.

Table 3. The average Standard Deviation (SD) and Coefficient of Variation (CV) values of the elements detected on the workpiece samples after treatment with different CuO concentrations

CuO(g)	Element	Mean (at.%)	SD (± at.%)	CV (%)	Level of Homogeneity
0	O	10.47	±7.01	66.90%	Not homogeneous
	Ni	0.034	±0.047	140.20%	Very non-homogeneous
0.25	O	≈ 13.0	≈ 16.6	128	Very non-homogeneous
	Ni	≈ 0.26	≈ 0.13	50	Moderate homogeneity
	Cu	≈ 0.27	≈ 0.30	111	Not homogeneous
0.5	O	≈ 9.72	≈ 13.6	140	Very non-homogeneous
	Ni	≈ 8.70	≈ 22.7	261	Very non-homogeneous
	Cu	≈ 0.38	≈ 0.38	~100	Not homogeneous
0.7	O	7.31	12.6	172	Very non-homogeneous
	Ni	19.66	31.8	162	Very non-homogeneous
	Cu	0.65	0.33	51	Moderate homogeneity

Homogeneity of O, Ni, and Cu elements was statistically estimated by means of mean, Standard Deviation (SD), and Coefficient of Variation (CV) with the EDX method at eight times in each CuO concentration (Table 3). Overall, for all tests, oxygen has a relatively high CV (>65%) (including CuO), which indicates inhomogeneous oxygen distribution (without CuO and for CuO-containing samples at a composition of 0.25–0.7 g). Because the sample was prepared in a laboratory with local oxides or contaminated surfaces, this could result in inhomogeneity due to local oxide generation, agglomeration of CuO particles, variations in coating thickness, or oxidation by the environment at the surface [4]. Nickel had a more pronounced trend of CuO concentration, possibly due to greater Ni exposure (due to uneven delivery of CuO or localized CuO deposits). But if Ni is further concentrated on the surface, then higher Ni CV values (~0.5 g and 0.7 g CuO >150%) may imply that Ni exposure leads to less positive coherence. By contrast, the dispersion of Cu was homogenous at 0.7 g CuO, which resulted in a CV value of ~51%, the greatest consistency of all possible Cu dispersion across all variants. However, the high oxygen variations mean that the CuO layer is not entirely continuous or homogeneous; therefore, there is no uniformity, and thus the detection of Cu and O from different measurement locations is not at a constant level. The results mostly verify that the homogeneity of the layers is not a definite thing, as CuO concentration increases, but the uniformity is obtained not only through depositional mode, particle agglomeration, but also the interaction of Ni and CuO layers in ASTM A36 steel substrate [32, 33].

3.9. Electrochemical Process

The electrochemical reactions of the workpiece are primarily initiated by anodic (metal oxidation), cathodic (species reduction in the environment), and ion and electron transport mechanisms linking the two reactions. In general, by the occurrence of these three mechanisms together, the surface corrosion size and extent depend on these mechanisms [34-36]. Therefore, the state and quality of the applied barrier have a significant effect on the state of the electrochemical reaction position.

The ASTM A36 steel in this application form may be subjected to a direct application to HCl solution unless an established protective coating has already been applied, which is an existing electroplated nickel or CuO coating with no other coating. (1) The electrochemical corrosion reactions, where nickel or CuO is put onto both surfaces and on the same surface (HCl solution) in the ASTM A36 steel system, are as shown in Figure 8. The reactions, in essence, can occur in one of three ways:

3.9.1. ASTM A36 Steel (Sample) Corrosion

When pores, cracks, or delamination are also found on the substrate of the Ni-CuO coating, the HCl mixture can go to the CS- ASTM A36 substrate. In the event that iron has such a structure, anode generation or even the presence of active dissolution may occur, which will cause corrosion, such as pitting or underfilm corrosion [34, 37]. In addition, because nickel (in relation to iron) has a higher electrochemical potential than iron (Equations 5–7), a metal layer of nickel can accelerate corrosion of the steel by means of galvanic coupling.

Anodic reaction (iron oxidation):

$$Fe \rightarrow Fe^{2+} + 2e^{-} \quad (5)$$

Cathodic reaction (hydrogen ion reduction):

$$2H^{+} + 2e^{-} \rightarrow H_2 \uparrow \quad (6)$$

Overall reaction:

$$Fe + 2HCl \rightarrow FeCl_2 + H_2 \uparrow \quad (7)$$

3.9.2. Corrosion of the Nickel Layer Due to Electroplating from the Electroplated Nickel Layer

Disruption or dissolution of the CuO layer will directly expose an underlying Ni layer to the HCl solution that directly comes into contact with the HCl solution. While Ni had higher corrosion resistance than Fe, Ni has poor resistance to strong acidity [30, 38], with dissolution being increasingly evident in high corrosion capacity. In this case, the Ni layer acts as a protective layer (i.e., limited sacrificial layer), but when it degrades in an aggressive medium, the Ni surface immediately influences the steel substrate, greatly increasing its rate of attack (Equations 8-10).

Anodic reaction (nickel):

$$Ni \rightarrow Ni^{2+} + 2e^{-} \quad (8)$$

Cathodic reaction:

$$2H^{+} + 2e^{-} \rightarrow H_2 \uparrow \quad (9)$$

Overall reaction:

$$Ni + 2HCl \rightarrow NiCl_2 + H_2 \uparrow \quad (10)$$

3.9.3. Reactions in the CuO Layer (Outermost Layer)

Although CuO is considered semi-passive, under strong acid stress, it can chemically dissolve instead of corroding on an electrochemical basis. The CuO layer is neither the primary anode nor cathode in the electrochemical reaction, of course, but it has been thought of as a physical barrier preventing corrosion-driven species from entering the atmosphere, and its protective activity is thus mostly down to thickness and consistency level. As this CuO layer dissolved in an acidic medium, a new coating of the Ni layer below may become exposed, and the corrosion process of the Ni layer could be accelerated [39, 40]. The chemical dissolution of CuO in HCl can be expressed in Equation 11:

$$CuO_{(s)} + 2H^{+} + 2Cl^{-} \rightarrow Cu^{2+} + 2Cl^{-} + H_2O \quad (11)$$

The proposed electrochemical reactions of the plated Ni–CuO metal in HCl solution for three environments (direct exposure to metal (a), nickel plating dissolving (b), and the exposure of the CuO layer (c)) are shown in Figure 8.

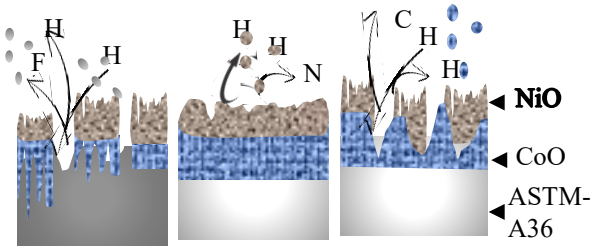

Fig. 8 schematically shows the electrochemical reactions occurring in the metal layer, electroplated Ni–CuO in HCl solution: Metal exposed directly to corrosive media (a), Nickel exposed to corrosive media (b), and (c) CuO layer exposed to corrosive media.

4. Conclusion and Future Works

Nickel-coated ASTM A36 steel with electroplating and CuO nanocoolant, dosed and applied at the concentrations of 0.25%, 0.5%, and 0.7%, respectively, showed improved surface characteristics with increasing CuO dissolution. Higher concentrations of CuO (0.7) yield approximately 9% increase in surface hardness. Corrosion was 50% lower than that of untreated steel in these environments. In EDX analysis, it is demonstrated that the elemental distribution for 0.7% CuO is more homogeneous (CV less than 50%), whereas the formation of coatings exhibited larger inhomogeneities and lower numbers of them (CV greater than 100%). The 0.7% CuO coating had a finer-grained, continuous, and somewhat homogeneous microstructure with smaller porosity and reduced particle agglomeration. In this case, however, the coating is degraded by three mechanisms: 1) in direct contact with the steel substrate; 2) corrosion of the nickel layer (which causes deposition of

CuO layer); and 3) dissolution or breakdown of the CuO layer in aggressive media. Compared to Ni–Co–P coatings, the inclusion of 0.5 wt% CuO nanoparticles enhanced hardness by 20% and improved adhesion strength. This enhancement is due to the nanoparticles promoting a denser microstructure and reducing internal defects during electrodeposition. To achieve a clear understanding of the relationship between structure and performance. Recent trends in CuO electroplating analysis focus on integrated characterization to link structure and performance. Techniques such as high-resolution SEM/EDX, advanced XRD, XPS, and electrochemical methods (EIS, Mott–Schottky) are used to evaluate morphology, phase purity, chemical states, and corrosion behavior. This approach enables better optimization of deposition parameters and coating functionality.

Acknowledgment

The authors are grateful to INTI International University for its assistance in this research. Special mention is also given to UNISKA and the Ministry of Education of Indonesia (DIKTI) (under contract numbers: 132/C3/DT.05.00/PL/2025, 18/LL11/KM/2025, and 158/UNISKA-LP2M/VI/2025) for providing materials and to all researchers who contributed towards the delivery of this work.

Conflicts of Interest

The authors acknowledge the non-conflicting role of their parties in this manuscript's publication. The research was performed individually without any financial or personal connections to the data that could have impacted the results or conclusions provided.

References

[1] *ASTM A36/A36M-19: Standard Specification for Carbon Structural Steel*, ASTM International, 2019. [CrossRef] [Google Scholar] [Publisher Link]

[2] ASM International, *Properties and Selection: Irons, Steels, and High-Performance Alloys*, ASM Handbook Committee, 1990. [CrossRef] [Google Scholar] [Publisher Link]

[3] George E. Totten, *Steel Heat Treatment Handbook*, 2006. [Google Scholar] [Publisher Link]

[4] William D. Callister, and David G. Rethwisch, *Materials Science and Engineering: An Introduction*, 10th ed., Wiley, pp. 1-944, 2020. [Google Scholar] [Publisher Link]

[5] J. R. Davis, *Metals Handbook Desk Edition*, 2nd ed., ASM International, 1998. [CrossRef] [Google Scholar] [Publisher Link]

[6] Balázs Illés et al., "Effects of CuO Nanoparticles on SAC Composite Solder Joints: Microstructural and DFT Study," *Journal of Materials Research and Technology*, vol. 32, pp. 609-620, 2024. [CrossRef] [Google Scholar] [Publisher Link]

[7] Rui Wang et al., "Study of the Microstructure and Corrosion Properties of a Ni-Based Alloy Coating Deposited onto the Surface of Ductile Cast Iron Using High-Speed Laser Cladding," *Materials*, vol. 15, no. 5, pp. 1-14, 2022. [CrossRef] [Google Scholar] [Publisher Link]

[8] Dana H. Abdeen et al., "A Review on the Corrosion Behaviour of Nanocoatings on Metallic Substrates," *Materials*, vol. 12, no. 2, pp. 1-42, 2019. [CrossRef] [Google Scholar] [Publisher Link]

[9] Shama Rehman, A. Mumtaz, and S. K. Hasanain, "Size Effects on the Magnetic and Optical Properties of CuO Nanoparticles," *Journal of Nanoparticle Research*, vol. 13, pp. 2497-2507, 2011. [CrossRef] [Google Scholar] [Publisher Link]

[10] Sifan Tan et al., "Study on Electrochemical Corrosion Behavior and Damage Repair Performance of Ni-La Composite Microalloyed Sn-Ag-Cu Solder Alloys at High Strain Rates," *Electrochimica Acta*, vol. 543, 2025. [CrossRef] [Google Scholar] [Publisher Link]

[11] Mai Van Phuoc, and Le Thi Phuong Thao, "Effect of CeO2 and CuO Oxide Nanoparticles on the Nickel Electroplating in Sulfate Solution," *Journal of Military Science and Technology*, vol. 107, no. 107, pp. 51-57, 2025. [CrossRef] [Google Scholar] [Publisher Link]

[12] S. Ayesha Barsanaa, A. Sultan Nasar, and M.J. Umapathy, "Enhanced Corrosion Resistance of Zinc Phosphate Coatings on Mild Steel through Incorporation of Nanocrystalline CeO_2 and CeO_2–CuO Nanocomposite," *RSC Advances*, vol. 15, pp. 20916-20934, 2025. [CrossRef] [Google Scholar] [Publisher Link]

[13] Kamelia Kamburova et al., "Hybrid Zinc Coating with CuO Nanocontainers Containing Corrosion Inhibitor for Combined Protection of Mild Steel from Corrosion and Biofouling," *Coatings*, vol. 12, no. 9, pp. 1-16, 2022. [CrossRef] [Google Scholar] [Publisher Link]

[14] Khazaal Hameed Khazaal, Omar A. Alwash, and Abbas Mezaal Karafe, "Environmentally Sustainable Alkyd-Based SiO_2–CuO Nanocoatings for Industrial Corrosion Protection: Synergistic, Structural, and Electrochemical Evaluation," *Annales de Chimie - Science des Matériaux*, vol. 49, no. 2, pp. 163-175. [CrossRef] [Google Scholar] [Publisher Link]

[15] Sachin Dua et al., "Conjugated Polymer-based Composites for Anti-Corrosion Applications," *Progress in Organic Coatings*, vol. 188, 2024. [CrossRef] [Google Scholar] [Publisher Link]

[16] Dmitry V. Dzhurinskiy et al., "Surface Modification of Aluminum 6061-O Alloy by Plasma Electrolytic Oxidation to Improve Corrosion Resistance Properties," *Coatings*, vol. 11, no. 1, pp. 1-13, 2021. [CrossRef] [Google Scholar] [Publisher Link]

[17] Pengxiang Lv et al., "Enhancement of Antimicrobial Properties of Plasma Electrolytic Oxidation Coatings on Aluminum Alloy Surfaces with CuO Nanoparticles," *Ceramics International*, vol. 50, no. 24, pp. 55449-55460, 2024. [CrossRef] [Google Scholar] [Publisher Link]

[18] Amal M. Abdel-karim et al., "Ag-CuO/epoxy Hybrid Nanocomposites as Anti-corrosive Coating and Self-cleaning on Copper Substrate," *Scientific Reports*, vol. 13, pp. 1-14, 2023. [CrossRef] [Google Scholar] [Publisher Link]

[19] Wang Heying et al., "Construction and Corrosion Resistance of Micro-arc Oxidation/CuO Nanoparticles/Polyurethane Composite Coatings on Magnesium Surface," *Surface Technology*, vol. 54, no. 15, pp. 108-119, 2025. [CrossRef] [Google Scholar] [Publisher Link]

[20] Haifeng Tan et al., "Effect of Current Density on the Corrosion Resistance and Photocatalytic Properties of Cu-Ni-$Zn_{0.96}Ni_{0.02}Cu_{0.02}O$ Nanocomposite Coatings," *Materials*, vol. 16, vol. 14, pp. 1-14, 2023. [CrossRef] [Google Scholar] [Publisher Link]

[21] *ASTM G1: Standard Practice for Preparing, Cleaning, and Evaluating Corrosion Test Specimens*, pp. 1-18, 2025. [Google Scholar] [Publisher Link]

[22] *ASTM G31–12A: Standard Guide for Laboratory Immersion Corrosion Testing of Metals*, ASTM International, 2012. [Google Scholar] [Publisher Link]

[23] *ASTM E92–17: Standard Test Methods for Vickers Hardness and Knoop Hardness of Metallic Materials*, ASTM International, 2017. [Google Scholar] [Publisher Link]

[24] Raymond H. Myers, Douglas C. Montgomery, and Christine M. Anderson-Cook, *Response Surface Methodology: Process and Product Optimization using Designed Experiments*, Wiley, pp. 1-856, 2016. [Google Scholar] [Publisher Link]

[25] George E.P. Box, J. Stuart Hunter, and William G. Hunter, *Statistics for Experimenters: Design, Innovation, and Discovery*, 2nd ed., John Wiley & Sons, pp. 1-672, 2005. [Google Scholar] [Publisher Link]

[26] Ryszard Rokicki et al., "Towards a Better Corrosion Resistance and Biocompatibility Improvement of Nitinol Medical Devices," *Journal of Materials Engineering and Performance*, vol. 24, pp. 1634-1640, 2015. [CrossRef] [Google Scholar] [Publisher Link]

[27] Robert Mašovic et al., "Investigation of Effect of Surface Modification by Electropolishing on Tribological Behaviour of Worm Gear Pairs," *Lubricants*, vol. 12, no. 12, pp. 1-18, 2024. [CrossRef] [Google Scholar] [Publisher Link]

[28] Feroze Nazneen et al., "Electropolishing of Medical-Grade Stainless Steel in Preparation for Surface Nano-Texturing," *Journal of Solid State Electrochemistry*, vol. 16, pp. 1389-1397, 2012. [CrossRef] [Google Scholar] [Publisher Link]

[29] Kai Feng et al., "Electropolishing of 316L Stainless Steel Small-Diameter Tubes: Reduced Surface Roughness and Enhanced Corrosion Resistance," *Journal of Materials Engineering and Performance*, vol. 34, pp. 13697-13709, 2025. [CrossRef] [Google Scholar] [Publisher Link]

[30] R. B. Rebak, *Uhlig's Corrosion Handbook*, 3rd ed., Wiley, 2011. [CrossRef] [Google Scholar] [Publisher Link]

[31] Benu Chatterjee, "Science and Industry of Electropolishing," *Galvanotechnik*, pp. 77-93, 2015. [Google Scholar]

[32] E. Arulkumar, S. Thanikaikarasan, and Nega Tesfie, "Influence of Deposition Parameters for Cu2O and CuO Thin Films by Electrodeposition Technique: A Short Review," *Journal of Nanomaterials*, vol. 2023, pp. 1-19, 2023. [CrossRef] [Google Scholar] [Publisher Link]

[33] Shaohua Wang et al., "Electrodeposition Mechanism and Characterization of Ni-Cu Alloy Coatings from a Eutectic-based Ionic Liquid," *Applied Surface Science*, vol. 288, pp. 530-536, 2014. [CrossRef] [Google Scholar] [Publisher Link]

[34] R. Winston Revie, and Herbert H. Uhlig, *Corrosion and Corrosion Control: An Introduction to Corrosion Science and Engineering*, Wiley, 2008. [CrossRef] [Google Scholar] [Publisher Link]

[35] T. Hryniewicz, K. Rokosz, and R. Rokicki, "Electrochemical and XPS Studies of AISI 316L Stainless Steel after Electropolishing in a Magnetic Field," *Corrosion Science*, vol. 50, no. 9, pp. 2676-2681, 2008. [CrossRef] [Google Scholar] [Publisher Link]

[36] Ojo S.I. Fayomi et al., "Development and Evaluation of Modified ZnCr-Shell Particulates Composite Coatings: Corrosion, Structural, and Microhardness Properties, *Hybrid Advances*, vol. 11, pp. 1-8, 2025. [CrossRef] [Google Scholar] [Publisher Link]

[37] Delstar Metal Finishing, Inc. (Houston, Tex.), *Electropolishing: A User's Guide to Applications, Quality Standards and Specifications*, Delstar, 2003. [Publisher Link]

[38] Pierre R. Roberge, *Corrosion Engineering*, McGraw-Hill, 2008. [Google Scholar] [Publisher Link]

[39] Mei Wen, and Karel Dušek, *Protective Coatings: Film Formation and properties*, 1st ed., Springer Cham, 2017. [CrossRef] [Google Scholar] [Publisher Link]

[40] Shahariar Chowdhury et al., "Structural and Morphological Properties of Aluminum-Doped Reduced Graphene Oxide Nanomaterials," *Materials Science and Technology*, 2025. [CrossRef] [Google Scholar] [Publisher Link]